



**HAL**  
open science

## Plant root growth against a mechanical obstacle: the early growth response of a maize root facing an axial resistance is consistent with the Lockhart model

Manon Quiros, Marie-Béatrice Bogeat-Triboulot, Etienne Couturier, Evelyne Kolb

### ► To cite this version:

Manon Quiros, Marie-Béatrice Bogeat-Triboulot, Etienne Couturier, Evelyne Kolb. Plant root growth against a mechanical obstacle: the early growth response of a maize root facing an axial resistance is consistent with the Lockhart model. *Journal of the Royal Society Interface*, 2022, 19 (193), 10.1098/rsif.2022.0266 . hal-03860136

**HAL Id: hal-03860136**

**<https://hal.science/hal-03860136>**

Submitted on 18 Nov 2022

**HAL** is a multi-disciplinary open access archive for the deposit and dissemination of scientific research documents, whether they are published or not. The documents may come from teaching and research institutions in France or abroad, or from public or private research centers.

L'archive ouverte pluridisciplinaire **HAL**, est destinée au dépôt et à la diffusion de documents scientifiques de niveau recherche, publiés ou non, émanant des établissements d'enseignement et de recherche français ou étrangers, des laboratoires publics ou privés.



Distributed under a Creative Commons Attribution 4.0 International License

### Abstract

Plant root growth is dramatically reduced in compacted soils, affecting the growth of the whole plant. Through a model experiment coupling force and kinematics measurements, we probed the force-growth relationship of a primary root contacting a stiff resisting obstacle, that mimics the strongest soil impedance variation encountered by a growing root. The growth of maize roots just emerging from a corseting agarose gel and contacting a force sensor (acting as an obstacle) was monitored by time-lapse imaging simultaneously to the force.

The evolution of the velocity field along the root was obtained from kinematics analysis of the root texture with a PIV derived-technique. A triangular fit was introduced to retrieve the elemental elongation rate or strain rate. A parameter-free model based on the Lockhart law quantitatively predicts how the force at the obstacle modifies several features of the growth distribution (length of the growth zone, maximal elemental elongation rate, velocity) during the first 10 minutes. These results suggest a strong similarity of the early growth responses elicited either by a directional stress (contact) or by an isotropic perturbation (hyperosmotic bath).

# Plant root growth against a mechanical obstacle: The early growth response of a maize root facing an axial resistance agrees with the Lockhart model

Manon Quiros<sup>1</sup>, Marie-Béatrice Bogeat-Triboulot<sup>2</sup>, Etienne  
Couturier<sup>3</sup>, and Evelyne Kolb<sup>1</sup>

<sup>1</sup>PMMH, CNRS, ESPCI Paris, Université PSL, Sorbonne  
Université, Université de Paris, F-75005, Paris, France

<sup>2</sup>Université de Lorraine, AgroParisTech, INRAE, UMR Silva,  
54000 Nancy, France

<sup>3</sup>Laboratoire Matière et Systèmes Complexes, Université Paris  
Diderot CNRS UMR 7057, 10 Rue Alice Domont et Léonie  
Ducquet, 75205 Paris Cedex 13, France

May 10, 2022

## 1 Introduction

### 1.1 Background

Plant roots uptake the water and nutrients required to satisfy the shoot demand. They also insure the mechanical anchorage of the plant in the soil to provide a stable basis for the shoot emergence and for its resistance to external loads due for example to wind blowing, soil erosion or shallow landslides [Gardiner et al., 2016], [Stubbs et al., 2019].

The root system architecture, that is the three-dimensional spatial arrangement of the different root types, derives from branching and growth of individual roots, that continuously sense and adjust their growth according to their local environment [Rellan-Alvarez et al., 2016]. In addition to environmental cues like water or nutrient availability, changes in branching, growth rate or growth direction depend on the mechanical stresses experienced by the growing roots [Gregory, 2006]. In particular, the root growth velocity decays with increasing soil strength, resulting in a reduced total root length and poor above-ground development [Tracy et al., 2011]. Typically for maize, the root growth velocity

was reduced by 50% when the soil resistance measured with a mini-penetrometer increased from 0.2 to 2 MPa [Veen and Boone, 1990]. For all species, root elongation stops when soil strength is too large.

In the current context of climate change, the frequency of extreme wet/dry and freeze/thaw cycles can exacerbate the compaction of soils and increase their strength, thereby limiting crop yield [Bengough et al., 2011]. As a consequence, breeding programs for plant species of agronomic interest such as wheat, soybean, rice or maize have been developed in soil science and ecophysiology communities to identify which root traits give the better plant fitness in large strength soils [Lynch et al., 2022], [Griffiths et al., 2022]. In particular, some works focused on macroscopic traits such as the number of root axes or the root tortuosity in relation with soil strengths [Colombi and Keller, 2019], [Popova et al., 2016], [Gregory et al., 2009]. However the underlying mechanisms at the root apex scale when the root tip encounters a hard pan, a compacted soil horizon or simply a rigid stone and experiences a huge resisting force, are still poorly understood. One of the main difficulty arises from getting reliable spatio-temporal information of root growth in opaque soils.

From a more fundamental point of view, the question arose as to quantify the maximum growth pressure, ie. the maximum axial stress a root is capable to exert on a resisting obstacle in different species. The assumption behind these studies was that roots having greater growth pressure might more easily penetrate stronger soil layers and access to water and nutrient pools. Interestingly the first measurements of axial force generated by growing roots were done by Pfeffer as earlier as 1893 [Pfeffer, 1893] and reproduced long after by Gill et al. (1995) [Gill and Bolt, 1955] and Souty [Souty, 1987]. More recently, different techniques such as calibrated spring system, elastic beams, or digital balances have been used (cited in Clark et al. (1999) [Clark et al., 1999]) to measure root axial pushing forces in model experimental systems. By dividing the maximum force value by the root cross section, growth pressures  $\sigma_{Max}$  of the order of 0.1 to 1 MPa have been obtained and were always in the range of the turgor pressure, that is the inner hydrostatic pressure inside the plant cells [Tracy et al., 2011], [Jin et al., 2013], [Potocka and Szymanowska-Pulka, 2018]. However the precise values of  $\sigma_{Max}$  appeared to vary with the species, but also with the protocol for root growth and measurements. In particular,  $\sigma_{Max}$  depended on the way the root tip was anchored or on the location and the time of root diameter measurements [Kolb et al., 2017]. Indeed feedback processes due to active root responses to confining geometries could occur within different time scales. [Bengough et al., 1997].

In this context, real-time information on the growth processes are needed but until now only very few studies recorded both force and strain rate field [Bizet et al., 2016] and had high temporal resolution to detect potential rapid biological responses.

## 1.2 Root growth

Primary root growth, that is root elongation, occurs in a so-called extended 'growth zone' located behind the root tip. This growth zone includes a meristematic zone where cells proliferate and an elongation zone where cells rapidly expand [Youssef et al., 2018]. The cells reaching the transition zone between the meristem and the elongation zone, leave their meristematic state and expand rapidly, increasing their volume by up to two hundred times. In addition, cell expansion is strongly anisotropic, leading to the characteristic cylindrical shape of the root. The plant cell is delimited by an hemi-permeable membrane surrounded by a rigid cell wall. The imbalance of osmotic pressures between the inside and the outside of the cell, on either side of the hemipermeable membrane results in an internal hydrostatic pressure, coined turgor pressure (or simply turgor). This pressure puts the cell wall under tension which might positively regulate cell expansion. Furthermore, the hydraulic conductivity of the cell membrane and the viscoplastic properties of the cell wall control the cell expansion rate [Cosgrove, 1987]. As modelled by Lockhart (1965) [Lockhart, 1965], growth is limited both by the cell wall properties and by the water uptake controlled by the hydraulic conductivity of the cell membrane [Cosgrove, 1987].

In roots, however, the membrane hydraulic conductivity appeared not to be limiting cell expansion and thus the growth rate appears to mostly depend on the cell wall properties [Pritchard, 1994]. The cell wall is under the tension produced by the turgor pressure and deforms irreversibly when the tension exceeds a yield threshold. Conversely the growth velocity is proportional to the turgor pressure in excess of a critical value.

Along the root apex, growth can be quantitatively described by the axial strain rate, also called the element elongation rate *EEER* [Silk and Erickson, 1979] [Baskin, 2013]. Kinematics analysis provides the velocity field and its spatial derivative gives the strain rate field [Silk and Erickson, 1979]. Thus, kinematics experiments are a non-destructive way to obtain the local growth distribution, including the growth zone length (from the location where the local strain rate is non zero) as well as the the maximum strain rate.

## 1.3 Root growth in impeding soil

In the presence of an impeding soil, root growth decreases with increasing soil strength. To include the effects of soil strength on root growth velocity, soil scientists proposed to consider the external resisting pressure of the soil as simply increasing the yield threshold for growth [Greacen and Oh, 1972]. If the derived phenomenological laws give the trends for growth velocity decaying with soil strength, the underlying assumptions are questionable and the force balance equations need to be rationalized. In particular it is not clear what soil stress should be incorporated inside the derived Lockhart-equations, as in situ measurements probe the soil strength resisting to the penetration of a penetrometer

and do not probe the external resisting stress really experienced by the root tip during root growth. Moreover the parameters such as turgor pressure, cell wall extensibility or yield threshold usually involved in Lockhart models are physiological quantities that are regulated over time by the root. They were shown to depend on the mechanical stress history of the root loading [Bengough et al., 1997].

In this work we address the question of how an external mechanical stress impacts the root growth rate by the use of a model experiment. We want to establish the force-velocity relationship to identify clearly how the growth process is modified with time when the root encounters a stiff obstacle and pushes against it. To answer this question, we built a new experimental setup combining force and kinematics measurements with a spatio-temporal analysis of the root growing against a force sensor acting as an obstacle. We chose a model species, maize, whose radicle has a typical diameter in the millimeter range and whose growth in the absence of mechanical stresses has been well characterized. Our analysis not only provides the root growth velocity but also fine kinematic parameters such as the growth zone extent and the local strain rate. These kinematic parameters are essential for characterizing the growth process and confronting them to growth models such as the Lockhart law [Lockhart, 1965].

## 2 Material and Methods

### 2.1 Experimental setup

The setup is made of a growth chamber mounted on a support with a movable part allowing the vertical adjustment of the force sensor just underneath the channel the root grew in. The growth chamber was made of two parallel glass plates (height 50 mm, width 70 mm) placed vertically and held together at a distance of 10 mm by an assembly of laser-cut Plexiglass walls (Figure 1a).

Agarose powder (2% w/v, SeaKem LE Agarose) was dissolved in de-ionized water at a temperature of 90°C, until becoming transparent. A small amount of the solution was then poured in the chamber, let to cool in order to seal the bottom edges, then the rest was poured in until the chamber was full. A graphite rod of calibrated diameter (0.7 mm) slightly smaller than the root's diameter ( $\approx 0.9$  mm) was inserted and maintained vertically in the middle of the cell until the agarose gel solidified. Afterwards, the graphite rod was removed, forming a vertical channel for the root to grow in (Figure 1b).

Maize seeds (variety P9874, Pioneer) were soaked in de-ionized water, aerated thanks to a bubbler for 24 hours, then were transferred to humid paper for 24 hours and held upright, root tip facing down in the direction of gravity. Seedlings with a 0.5 to 1 cm-long radicle were selected for the experiments. The radicle was carefully inserted in the channel at the top of the chamber, and the seed was maintained in place with a parafilm sheet. Vaseline was spread on

the bottom-exposed areas of the agarose gel to avoid water losses. Then the agarose-filled chamber was fixed on the support just over the force sensor. The setup allowed the simultaneous monitoring of the root growth (through the agarose gel) and of the root force when the radicle emerged from the gel and pushed again the force sensor. The root grew in the channel for around 19 hours and arrived vertically onto the force sensor, acting as an obstacle. Temperature was continuously monitored and experiments were conducted with temperatures in the range of  $\theta_0 \in [21^\circ C - 28^\circ C]$ . For each experiment with a given  $\theta_0$ , the standard deviation on  $\theta_0$  did not exceed  $0.5^\circ C$  during the time course of kinematics measurements. In this range, the 2% w/v agarose gel behaves as a stiff elastic material with an elastic modulus of around  $22.5 \pm 0.5 \text{ kPa}$  (measured with a HAAKE Rheometer, Thermofisher).

## 2.2 Force measurements

The force was measured thanks to a Futek (LSB200) force sensor, with a maximum range of 100 g and a stiffness of  $4828 \pm 5 \text{ N/m}$ . The signal was acquired at a frequency of 1000 Hz, then averaged every second during the whole experiment duration. In order to avoid the root tip slipping when contacting the force sensor, we fixed a rough sand-covered plexiglass rectangle on the top face of the force sensor. The sand particles (diameter  $\leq 350 \mu m$ ) were painted black to avoid any unwanted light reflections.

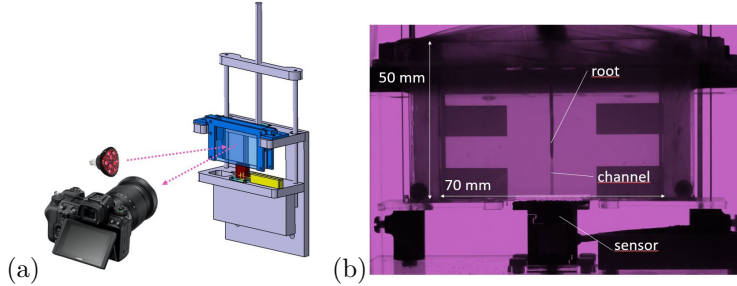


Figure 1: Experimental setup. (a) Schematic view: The agarose-filled cell (blue) is fixed on a support (grey). The vertical position of the force sensor (red) can be adjusted just at the outlet of the vertical channel guiding the root growth. A 3D-printed support (yellow) holds all the electrical wires. The input wires are connected externally (not shown) to a stabilized power supply and the output wires are connected to a LabView interface. A CCD camera saves the images of the root illuminated by an infra-red lighting.(b) Global view of the growth chamber with the transparent agarose gel filling the chamber and the maize root inside the vertical channel perpendicular to the horizontal surface of the force sensor.

## 2.3 Kinematics of root growth

### 2.3.1 Experimental observation and image processing

Root growth was monitored by time-lapse photography. The whole setup was illuminated with low angled Infra-Red lighting (IR,  $\lambda = 850nm$ ) (Figure 1a). This IR lighting has two advantages. First, root growth is not disturbed by phototropic effects that might occur with visible light. Second, IR lighting gives a texture to the root surface, that is, a pattern of bright points that can be followed along time to get the displacement field along the root [Youssef et al., 2018]. For this kinematics study of the root growth, we used a high-resolution CCD camera (Nikon D5200,  $4000 \times 6000$  pixels) whose IR absorbing filter was removed, with a macro lens (Nikkor 60 mm). The observation field was 25 mm in height with a typical resolution of  $4.7\mu m$  per pixel. When the root tip was entering the observation field and approaching the contact, the images were taken every minute during 15 hours.

Then, images were processed with Kymorod, a Matlab app developed by Bastien et al. (2016) [Bastien et al., 2016], that performed PIV (Particle Image Velocimetry) on the texture of elongating organs. Kymorod was run with a time lapse of 4 minutes between images. We recovered the raw displacement fields as a function of the curvilinear abscissa  $s$  along the root skeleton (Figure 2) and used a fitting procedure to determine the local velocity  $v_l$  and the strain rate (noted *EER* for Elementary Elongation Rate) profiles.

### 2.3.2 Velocity, Strain rate profiles and fitting procedures

Numerical derivation can be done in numerous ways by deriving local fits (splines) or global fits. To minimize the number of parameters and make the *EER* estimation the more robust possible, we chose the simplest global fit with the following constraints: The fit function for the strain rate profile  $EER(s)$  must have a finite support (for modelling the limited extent of the growth zone and the absence of growth elsewhere) and once spatially integrated, it should give a sigmoid shape similar to velocity profile. These conditions required that the fit function for  $EER(s)$  had to be an isosceles triangle :

$$s \rightarrow 2a(s - b)\mathbb{1}_{[b, b+c]} + (2a(b + 2c - s))\mathbb{1}_{[b+c, b+2c]}. \quad (1)$$

where  $\mathbb{1}_{[x, y]}$  is the function that is 1 in between  $x$  and  $y$  and 0 elsewhere and with  $a, b, c$  the three fit parameters describing the triangular shape. The function family (1) stands for triangle shape displacement profile whose height is the maximum strain rate  $EER_{max} = 2ac$  and whose base is the length of the growth zone  $L_{GZ} = 2c$  (see the triangular sketch of Figure 8).

Hence the velocity fit function family is obtained by spatial integration over  $s$  of the function (1):

$$s \rightarrow a(s - b)^2\mathbb{1}_{[b, b+c]} + (2ac^2 - a(s - b - 2c)^2)\mathbb{1}_{[b+c, b+2c]} + \mathbb{1}_{[b+2c, \infty]}[2ac^2 + d] \quad (2)$$

with 4 parameters only, one of which ( $d$ ) being due to integration. Other velocity fit functions were proposed in the literature [Peters and Baskin, 2006]; this



one was retained for having a finite support of the growth zone and only 4 parameters.

In this way, growth velocity  $v$  of the root is given by the maximum of the fit function (2):  $v = 2ac^2$ .

### 3 Experimental Results

#### 3.1 Growth before contact

The roots grew along the vertical channel inside the agarose gel. The water required for root growth was supplied by the gel surrounding the root and a drop of water probably released by the compressed gel was observed just at the root cap, preventing any dehydration of it. The root diameter being slightly larger than the channel, there was no air interface between the root and the gel, allowing a good IR specs visualization and PIV processing. After a transient regime of 2 hours during which the root growth velocity increased, a stationary regime was reached with a typical velocity of around 4 cm/day.

The imaging of the root with infra-red lighting and the subsequent analysis with the PIV analysis of Kymorod allowed to obtain the root skeleton (yellow line in Figure 2) and the local velocity profile  $v_l$  as a function of the curvilinear abscissa  $s$  along the root length. A typical example of this profile before the root contacts the obstacle is given in Figure 2, middle panel. The reference  $s = 0$  was arbitrarily set at the extreme point of the observation frame toward the seed. The velocity  $v_l$  increased from the curvilinear abscissa  $s = 14$  mm until the root tip at around  $s = 24$  mm (purple curve of the middle panel of Figure 2). The extent of this zone where  $v_l$  departs from zero corresponds the growth zone. The raw velocity field was fitted by equation (2). The fit function (black curve) nicely reproduced the experimental data. The maximum of this fit gave the root growth velocity  $v = 28.9 \mu m.min^{-1}$ . From this fitting procedure, we got the three fit parameters of equation (1) necessary to properly define the strain rate profile (bottom panel of Figure 2) and the growth parameters. Hence for this example before contact,  $L_{GZ} = 8.64$  mm and  $EER_{max} = 6.18 \times 10^{-3} min^{-1}$ .

We proceeded in the same way for all the roots investigated. The average growth velocity before contact was  $v = 28.5 \pm 2.5 \mu m.min^{-1}$ . The averaged growth zone length ( $L_{GZ}$ ) was  $8.9 \pm 0.6 mm$  and the averaged maximum strain rate ( $EER_{max}$ ) was  $5.9 \pm 0.6 \times 10^{-3} min^{-1}$ . Root growth velocity, growth zone length and maximum strain rates were similar to those already described in previous maize studies [Sharp et al., 1988], [Walter et al., 2003], indicating that our set-up with the root inserted in gel did not induce any oxygen deficiency nor affect root growth.

#### 3.2 Contact

After a typical duration of 19 hours inside the gel, the root tip reached the gel bottom and touched the force sensor with a normal incidence. The precise

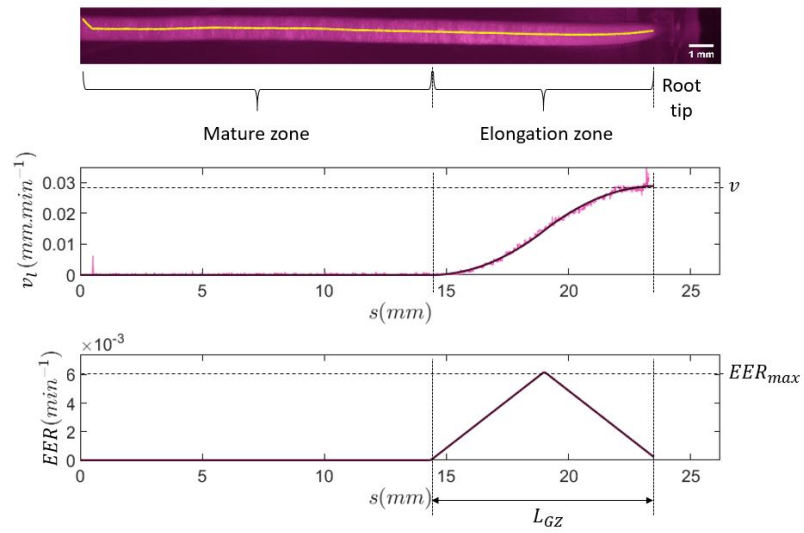


Figure 2: Top panel: Cropped and 90 degrees rotated image of the root apex (before contact) under IR lighting with the yellow skeleton obtained from Ky-morod analysis superimposed on it. Middle panel: Local velocity profile  $v_l$  along the root curvilinear abscissa  $s$  with raw data in purple and its fit in black line with its maximum, ie. the growth velocity  $v$ . Bottom panel: Strain rate ( $EER$ ) along the root abscissa  $s$  obtained by spatial derivation of the fitted velocity profile, with indications of  $L_{GZ}$  for the length of the growth zone and  $EER_{max}$  for the maximum strain rate.

determination of the contact time was challenging since the zone of root-sensor contact was blurred, due to the gel bottom-air interface, preventing a visual determination of the contact occurrence. Considering that the contact time did not necessarily coincide with the force increase, we used a method based on the spatio-temporal analysis of the displacements of the bright points of the root texture.

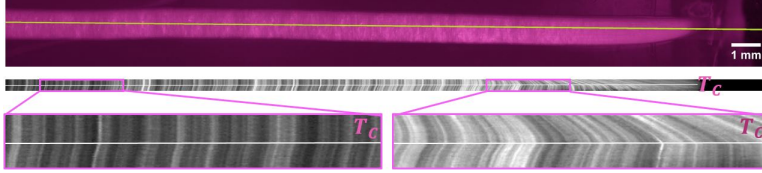


Figure 3: Spatiotemporal analysis of the root images. Top: picture of the maize root under IR lighting with the 1 pixel-thick straight line used as a slice for the spatio-temporal analysis. Middle: Full spatio-temporal image converted in gray-levels with increased contrast. The horizontal axis shows variations along the root, with the root cap on the right side. The vertical axis represents increasing times from top to bottom. Bottom images: zooms of the spatio-temporal in the mature zone (left) and in the growth zone (right). The white line indicates the slope break determining the time  $T_C$  when the root contacts the force sensor.

We draw a vertical line of 1 pixel width along the root on each IR image and analyzed the resulting spatio-temporal pattern. In Figure 3 the image of the root has been rotated by 90 degrees. In the middle and bottom panels each horizontal line corresponds to one slice along the root at a given time, and the vertical from top to bottom corresponds to increasing times, each slice being separated by 1 min. On the right part of the slices, the growth zone can be identified by the location of oblique lines (see the right zoom of the spatio-temporal in Figure 3): the progressive shift of the bright spots shows the displacement of cells along the root axis. The slope of these oblique lines increases from left to right due to the cumulative effect of local growth on the more apical cells of the root tip. In the mature zone (left zoom of Figure 3) where there is no growth, the bright points of the texture stay in place along time before contact, resulting in vertical lines in the spatio-temporal image. At time  $T_C$ , a slope break is observed in the vertical lines, the spots appear displaced backward toward the seed. As the force sensor was much more rigid than the root, the contact led to a backward movement of the IR specks that could result from a shortening of the mature zone due to compression or to a pullback of the whole seedling. We thus considered this event as due to the contact of the root tip with the force sensor. To determine  $T_C$ , isointensity lines of the spatio-temporal diagram were detected using the Contour function of Matlab; the longest ones (going from the initial to the final times of the spatio-temporal diagram) were selected; a piece-wise linear function with two pieces was fitted; the time  $T_C$  corresponded to the junction between these two pieces. Note that a second noticeable slope break occurred later when the root markedly bends.

### 3.3 Force build-up

Once the contact time was determined, we could precisely follow the evolution of force  $F$  as a function of the rescaled time  $t = T - T_C$ , for which we set  $F(t = 0) = 0$ . A typical evolution of the force  $F$  exerted by the root on the force sensor is plotted as a function of the rescaled time  $t$  (Figure 4) with insets corresponding to the images of the root and the computed skeletons (in yellow) at different characteristic times.

The force was observed to increase with time, as the root continued to grow and thus to push against the force sensor. From time  $t_I$  which denotes the time where the force started to increase noticeably, the signal evolved in a linear way until time  $t_L$ . The end of this linear regime was obtained mathematically following the successive steps below:

- Calculating linear fits for the portions of the  $F$  versus  $t$  curve beginning at  $t_I$  and ending at the successive times  $t$ .
- Calculating the successive quadratic distances between the portions of curve  $F$  versus  $t$  and the corresponding fits. Each quadratic distance is normalized by the corresponding  $t$ .
- Plotting the histogram of quadratic distances and identifying its first peak. This first peak corresponds to all the data where the linear fit was very close to the experimental force-time data. The location and width of this first peak are calculated by the matlab function `findpeaks` (`MinPeakHeight=40` and `MinPeakProminence=4`).  $t_L$  is given by the maximal time whose quadratic distance lays in the first peak of the histogram.

By this method, we determined for the typical example of Figure 4, a time  $t_L = 23.4$  min for a time  $t_I = 2.5$  min and a typical slope  $\frac{\Delta F}{\Delta t} = 3.9$  mN/min. When normalized by the initial root growth velocity  $V_0 = 28.9$   $\mu\text{m}/\text{min}$  we obtained a value of  $\frac{\Delta F}{\Delta t \times V_0} = k_{eff} = 135$  N/m, which has the dimension of an effective root stiffness ( $k_{eff}$ ).

Then after time  $t_L$ , the signal of force versus time rounded off until a maximum force value of around  $F_{max} = 0.11$  N was reached for this root. After this maximum force  $F_{max}$  was reached, there was a marked and spatially-extended bending of the root: the root axis appeared curved along a typical length of  $7.5 \pm 0.7$  mm (right inset of Figure 4). This event was thus associated to a macroscopic buckling of the root inside the gel.

The existence of a linear regime of force increase and then a rounding off of the force signal until a maximum force value were observed for all investigated roots. When averaged over  $n = 7$  roots, the duration of the linear regime was  $t_L - t_I = 15 \pm 4$  min and the characteristic slope was  $4.5 \pm 0.7$  N/min corresponding to an effective stiffness  $k_{eff} = 159 \pm 32$  N/m (the value following  $\pm$  is the standard deviation over  $n = 7$  roots).

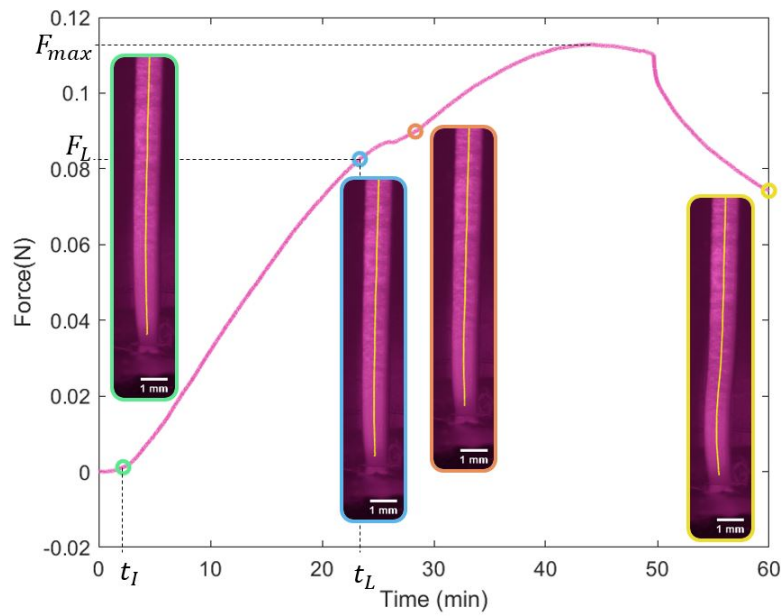


Figure 4: Force  $F$  as a function of time  $t$ .  $t = 0$  corresponds to the contact time. Characteristic times are indicated with dotted vertical lines: time  $t_I$  (resp.  $t_L$ ) is the beginning (resp. end) of the linear increase of force. Insets: pictures of the root at different characteristic times ( $t = 2.5, 23.4, 28.3$  and  $60$  min from left to right respectively).

### 3.4 Growth response

From the successive images and Kymorod analysis, we could follow the kinematics of root growth before and during the contact with the force sensor. The velocity profiles varying with time are represented with a 3D map in Figure 5 for the same root as in Figure 4. The white line is the velocity profile at the rescaled time  $t = 0$  corresponding to the contact with the force sensor ( $T_C$ ). Before contact, that is for times  $t < 0$ , the successive velocity profiles were similar with a growth zone starting at around  $s = 14$  mm and extending until  $s = 24$  mm. Small variations of the maximum velocity (that is the root growth velocity  $v$ ) are visible during the 30 min preceding the contact with a value of  $v$  in between 0.0278 mm/min and 0.031 mm/min. Once the root tip contacted the force sensor, we observed a drastic change of behaviour. The maximum velocity decayed rapidly over 15 minutes and then more gradually over the next 15 minutes. Growth monitoring by kinematics allowed to highlight that the root continued to grow although its tip was blocked by the rigid force sensor. This could not have been shown by a more classical method such root tip displacement monitoring. This also implies that the increase in root length was "dispersed" by either seed pullback, mature tissue compression or micro-bendings.

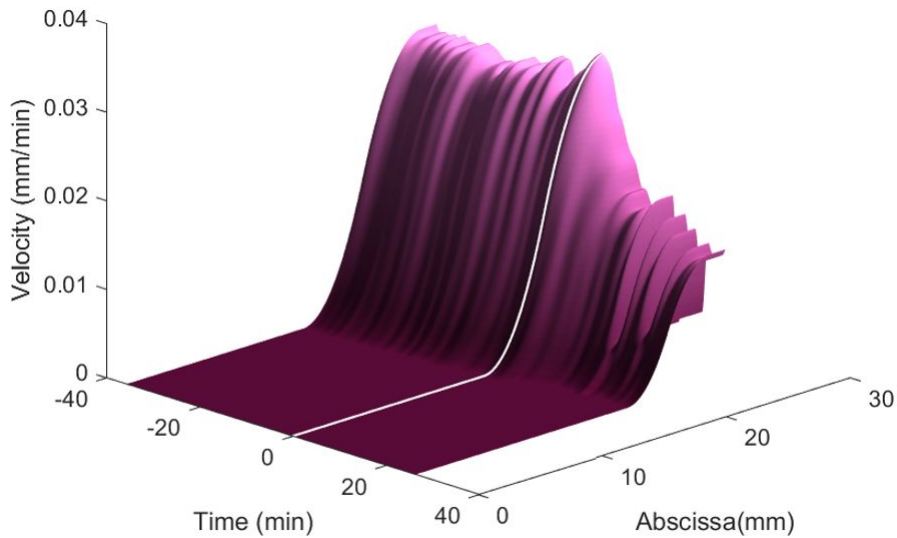


Figure 5: 3D map of the velocity profile  $v_l$  along the curvilinear abscissa  $s$  of the root skeleton for different times  $t$  before and after the contact (identified by the white line at  $t = 0$ ).

### 3.5 Coupling Force and Growth

The fitting procedures were applied to all the velocity profiles before and after the contact and gave the growth parameters shown in Figure 6. In particular, the growth velocity  $v$  was plotted as a function of time (top left panel in Figure 6). In the typical example, we could observe a quasi-linear decay of the growth velocity  $v$  over a duration of around 10 minutes after contact. Then the decay was slower and the growth did not stop in the represented time range. Note that we stopped the kinematic fitting procedure when the root clearly bent at time  $t_B = 40$  min. This bending did not necessarily occur in the observation plane, which does not allow to use the kinematics analysis beyond this time. The simultaneous acquisitions of force and IR images also allowed to plot the growth velocity as a function of force (top right panel in Figure 6). After a marked decay of velocity with increasing force until an amplitude of 0.04 N, the growth velocity seemed to decay much slower. Growth persisted even if the resisting force was still increasing.

Besides growth velocity, the fitting procedures also gave the growth zone length  $L_{GZ}$  (lower panels of Figure 6). Starting from  $L_{GZ} = 9$  mm well before contact, the growth zone length shrank rapidly to 6.5 mm after around 10 min then decayed more slowly. In a similar manner as the growth velocity,  $L_{GZ}$  also decayed with force, seemed to stabilize at 6.5 mm for a force level of 0.03-0.04 N, before a small rise and a further decrease down to 5.5 mm.

We proceeded to the same analysis for force and growth for the different roots and summarised in Figure 7. The growth velocity was normalized by its value  $V_0$  just before contact and the force  $F$  was divided by a constant force level of  $F_N = 0.04$  N corresponding to the levelling off of the velocity in the typical example. Despite the inherent biological variability of the seeds, the curves of the rescaled velocity  $V/V_0$  versus rescaled force  $F/F_N$  collapse rather well for the  $n = 7$  roots we measured.

## 4 Lockhart's law dictates root-obstacle interaction at short time scale

### 4.1 Model

We propose to interpret our experimental results in the framework of Lockhart law [Lockhart, 1965]. This law establishes a relationship between the strain rate at the cell scale and the turgor pressure inside the cell that puts the rigid cell wall under tension. The cell wall growth regulation by turgor follows the same numerical law as a Bingham fluid which deforms irreversibly above a yield stress : while turgor pressure  $P$  exceeds a given threshold in pressure, cell walls flow and expand. We recall that whereas  $P$  is isotropic, the primary cell walls are mechanically anisotropic.

We have adapted this approach to the case of a root encountering an obstacle for modelling the growth-force relationship. Notations and analysis are inspired

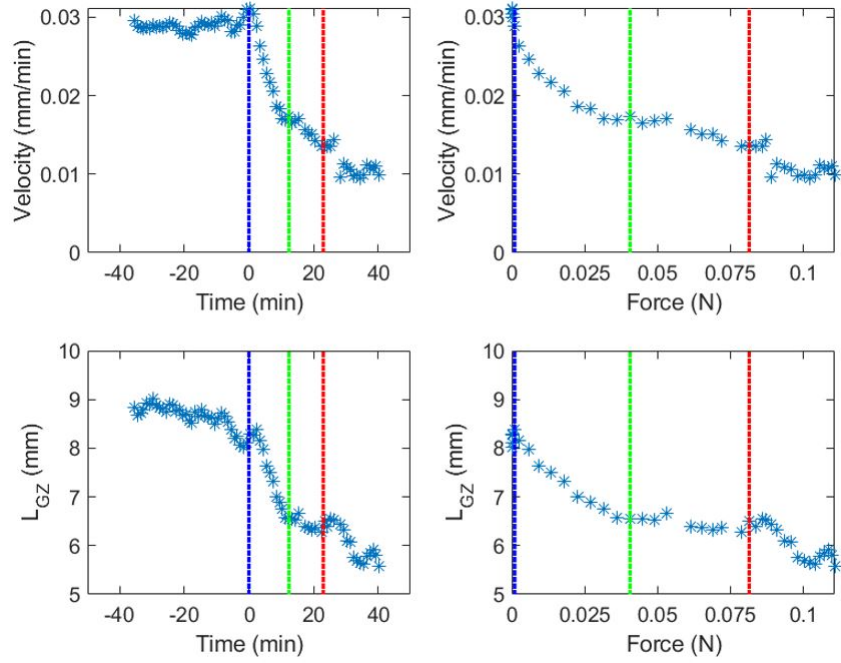


Figure 6: Growth parameters, ie. growth velocity  $v$  (top panels) and growth zone length  $L_{GZ}$  (bottom panels) obtained by fitting the velocity profiles  $v_l(s)$  with equation (2) for the same root as in Figure 5. Left panels: as a function of time  $t$ ,  $t = 0$  corresponding to the contact time (dotted line). Right panels: as a function of measured force  $F$ . The blue, green and red dotted lines represent respectively the contact time, the time corresponding to  $F = F_N = 0.04N$ , and the time  $t_L$  when the linear rise in force ends.



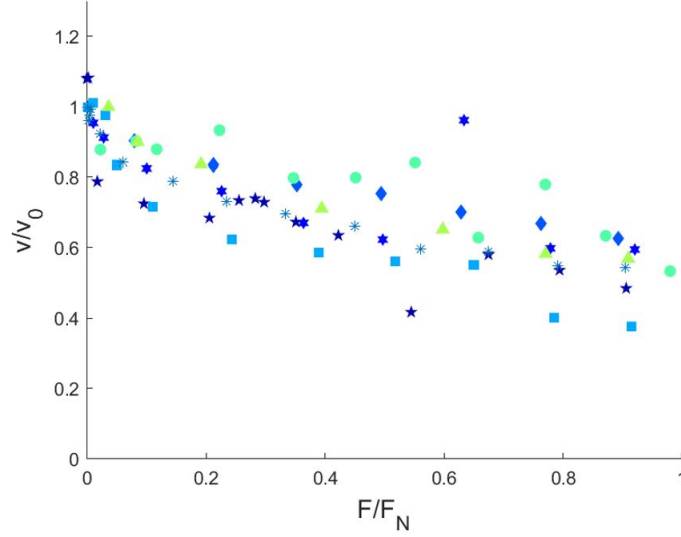


Figure 7: Velocity normalized by the initial velocity  $V_0$  just before contact as a function of the rescaled force  $F/F_N$  where  $F_N = 0.04 \text{ N}$  for the 7 different roots (one given symbol and color per root, the asterisks corresponding to the root described in the preceding figures).

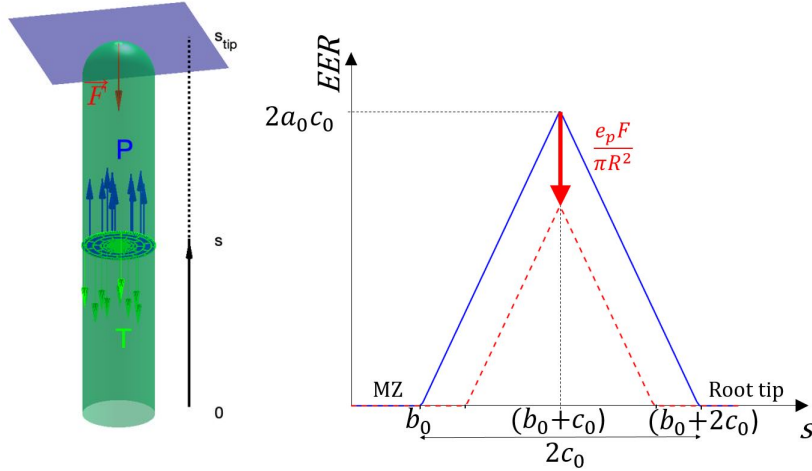


Figure 8: Sketch of a root.  $s$  is the curvilinear abscissa along the root. In the transversal cross-section at  $s$ :  $\mathcal{A}_{cytoplasm}$  (resp.  $\mathcal{A}_{wall}$ ) stands for the cross-sectional area of the cytoplasm (blue zone) (resp. cell wall (green zone)).  $P$  stands for the turgor pressure,  $T$  stands for the cell wall tension and  $F$  stands for the apical force.

by the work of Dyson et al. (2014) [Dyson et al., 2014].  $F$ , the force exerted at the root tip by the obstacle is balanced by the contributions of  $P$ , the turgor pressure, and  $T$ , the cell wall tension. Other environmental forces such as the frictional forces on the root flanks are neglected. The force balance applied to the root part laying between the  $s$  cross-section and the tip (See Figure 8) gives:

$$-F - \int_{wall} T \cdot dA_w + \int_{cytoplasm} P \cdot dA_c = 0. \quad (3)$$

The area of the  $s$  cross-section  $\mathcal{A}(s)$  being  $\pi [R(s)^2]$  can be decomposed in its cytoplasmic part  $\mathcal{A}_{cytoplasm}(s)$  (liquid part under turgor pressure  $P$ , in blue in the the left panel of Figure 8 and its cell-wall part  $\mathcal{A}_{wall}(s)$  (solid part under tension  $T$  in green in Figure 8 left):

$$\mathcal{A}(s) = \mathcal{A}_{wall}(s) + \mathcal{A}_{cytoplasm}(s).$$

Using  $\bar{T}$ , the tension averaged on the cell wall of the  $s$  cross-section and  $\bar{P}$ , the turgor averaged on the cytoplasmic area of the  $s$  cross-section, equation (3) rewrites:

$$-\mathcal{A}_{wall}\bar{T} + \mathcal{A}_{cytoplasm}\bar{P} - F = 0.$$

$\bar{T}$  is a simple function of  $\bar{P}$  and  $F$ :

$$\bar{T} = \frac{\mathcal{A}_{cytoplasm}\bar{P} - F}{\mathcal{A}_{wall}}. \quad (4)$$

Neglecting the tension variations over the  $s$  cross-section, the Lockhart equation expressing the strain rate  $EER(s, F)$  for an applied force  $F$  reads:

$$EER(s, F) = e_T(s) \left( \bar{T} - Y_T(s) \right)_+ \quad (5)$$

$e_T$  (resp.  $Y_T$ ) being the local extensibility (resp. the local threshold) expressed in tension. The subscript '+' indicates that the formula is valid if  $(\bar{T} - Y_T(s)) > 0$  and  $EER(s, F) = 0$  otherwise. Substituting (4) in (5) gives:

$$EER(s, F) = e_T(s) \left( \frac{\mathcal{A}_{cytoplasm}}{\mathcal{A}_{wall}} \bar{P} - Y_T(s) - \frac{F}{\mathcal{A}_{wall}} \right)_+. \quad (6)$$

The strain-rate profile before contact  $EER(s, 0)$  is given by the same equation (6) by setting  $F = 0$ . Then it is possible to rewrite the strain rate during contact  $EER(s, F)$  in the following way:

$$EER(s, F) = \left( EER(s, 0) - \frac{e_T(s)F}{\mathcal{A}_{wall}} \right)_+. \quad (7)$$

The extensibility  $e_T$  has been estimated indirectly by retrieving data points from Frensch and Hsiao (1995) who were studying the maize root growth submitted to water stress. Their data in Figure 7 of [Frensch and Hsiao, 1995]

showed the extensibility to decrease slowly from tip to base (Figure 7D) : the extensibility expressed in turgor was  $e_P = 2.36 \pm 0.7 \text{MPa}^{-1} \text{h}^{-1}$  ( $N = 3$ ), relative standard deviation 0.0545 ( $N = 3$ ), whereas the threshold profile followed a bell shape inversely correlated with the  $EEER$  profile (relative standard deviation 0.14 ( $N = 3$ )). These observations led us to suppose  $e_P$  to be constant along the growth zone and to explain the strain rate variation solely by the threshold variation:

$$EEER(s, F) = \left( EEER(s, 0) - \frac{e_P F}{\mathcal{A}_{cytoplasm}} \right)_+, \quad (8)$$

$e_T$  being converted in  $e_P$  according to:

$$e_T = (\mathcal{A}_{wall} / \mathcal{A}_{cytoplasm}) e_P.$$

Thus the strain rate profile at a given force  $F$  can be simply expressed as a linear combination of the force  $F$  and the strain-rate profile before contact:

$$EEER(s, F) = \left( EEER(s, 0) - \frac{e_P F}{\pi R^2} \right)_+, \quad (9)$$

where  $\mathcal{A}_{wall}(s)$  is neglected compared to  $\mathcal{A}_{cytoplasm}(s)$ , leading to  $\mathcal{A}_{cytoplasm}(s) \approx \pi [R(s)^2]$ .

Substituting the fit of  $s \rightarrow EEER(s, 0)$  with formula (1) in equation (9) gives:

$$EEER(s, F) = \left( 2a_0(s-b_0)\mathbb{1}_{[b_0, b_0+c_0]} + (2a_0(b_0+2c_0-s))\mathbb{1}_{[b_0+c_0, b_0+2c_0]} - e_P F / (\pi R^2) \right)_+. \quad (10)$$

The function  $s \rightarrow EEER(s, F)$  calculated with this formula is still triangle shaped with a height (Figure 8 right):

$$EEER_{max} = 2a_0c_0 - e_P F / (\pi R^2). \quad (11)$$

Then the growth zone length ( $L_{GZ}$ ) corresponding to the basis of the triangle  $s \rightarrow EEER(s, F)$  is easily obtained by noting that  $s \rightarrow EEER(s, F)$  and  $s \rightarrow EEER(s, 0)$  are two similar triangles:

$$L_{GZ} = 2c_0 \frac{2a_0c_0 - e_P F / (\pi R^2)}{2a_0c_0} \quad (12)$$

which simplifies in:

$$L_{GZ} = 2c_0 - \frac{e_P F}{a_0 \pi R^2}. \quad (13)$$

The growth velocity is given by the area of the triangle ( $s \rightarrow EEER(s, F)$ )

$$v = \frac{(2a_0c_0 - e_P F / (\pi R^2))^2}{2a_0}. \quad (14)$$

After substitutions with the parameters before contact  $L_{GZ,0}$ ,  $EER_{max,0}$  and  $v_0$ , the kinematic parameters after contact are:

$$L_{GZ} = L_{GZ,0} \left( 1 - \frac{e_P F}{\pi R^2 EER_{max,0}} \right). \quad (15)$$

and

$$v = v_0 \left( 1 - \frac{e_P F}{\pi R^2 EER_{max,0}} \right)^2. \quad (16)$$

Both the velocity and the growth-zone length can be predicted (Formula (15) and (16)) from the displacement profile before impact, the root radius and the force. The match between prediction and experimental data is good (Figure 9 a and b). Moreover the linear regression coefficient of the curve  $F$  vs  $(\pi R^2 EER_{max,0}) (1 - \sqrt{v/v_0})$  (resp.  $F$  vs  $(\pi R^2 EER_{max,0}) (1 - L_{GZ}/L_{GZ,0})$ ) lead to estimations of  $e_P$  both very close to each other ( $1.87 \pm 0.36 \text{ MPa}^{-1} \text{ h}^{-1}$  and  $1.87 \pm 0.52 \text{ MPa}^{-1} \text{ h}^{-1}$ ,  $N = 7$ ) and close from the measurements of [Frensch and Hsiao, 1995]  $2.36 \text{ MPa}^{-1} \text{ h}^{-1}$ .

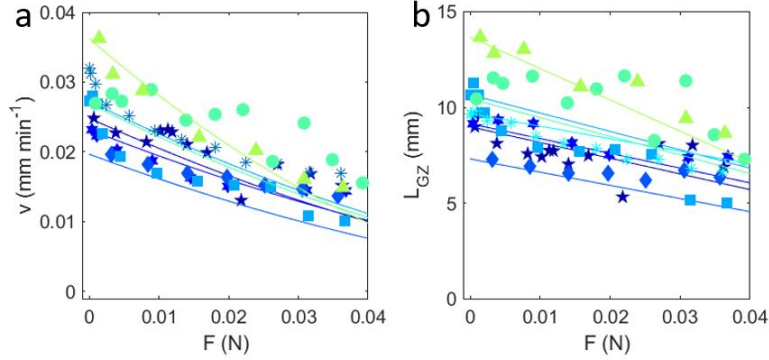


Figure 9: a. Force vs velocity. b. Force vs growth zone length. For both a and b, the circles are experimental points and the continuous lines are the theoretical predictions.

## 4.2 Discussion

Mechanical cues trigger lots of responses at different time scales [Landrein and Ingram, 2019]; the present data show that the first phase (ten first minutes or  $F < 0.04N$  between the blue and green vertical dotted lines on Figure 4) of the root growth response to an obstacle can be described with evolution laws derived from the Lockhart model. In this model, the strain rate ( $EER$ ) remained proportional to the wall tension (above a predetermined threshold), while the wall tension was decreasing due to the increasing force exerted at the root tip. After this first phase, the root growth velocity decreased more slowly

than expected from the model while the force kept increasing and finally reached a plateau (see Figure 6 between the green and red vertical dotted lines). In a third phase (after the red line of Figure 6 or after  $t_L$  in Figure 4), the force was no more linear with time and the velocity-force relationship was noisy. We interpret this phase as due to a localized bending allowing the dispersion of new tissue (produced by growth) transversely to the vertical axis. Note that the macroscopic bending corresponding to a clear buckling event happened later on and kinematics analysis were stopped there.

In the past, most tests of the Lockhart growth law were non-directional (i) by varying cell internal pressure either using a cell pressure probe [Zhu and Boyer, 1992] or varying external osmolarity [Frensch and Hsiao, 1995], or (ii) by applying an external pressure by use of a pressure chamber [Cosgrove, 1987] while monitoring growth. The reduction of cell wall tension by hyper-osmotic treatments was shown to elicit two homeostatic responses of the plant: a reduction of the growth threshold to come back to the initial growth rate coined "cell wall loosening" [Green et al., 1971] and an increase in internal osmolyte concentration to at least partially restore turgor, coined "osmotic adjustment". For instance, a maize root with an initial turgor of 0.67 MPa immersed in a 0.3 MPa mannitol solution (hyper-osmotic bath) ceased to grow very rapidly when the turgor decreased below 0.6 MPa [Frensch and Hsiao, 1994] suggesting an initial very high turgor threshold. Turgor reached a minimum (0.34 MPa) two minutes later after which it started to recover for 30 min by osmotic adjustment. Finally the growth was restored ten minutes later when the turgor was only 0.46 MPa, indicating cell wall loosening and a new decreased turgor threshold (0.46 MPa in comparison with 0.6 MPa). In a second experiment, after a lower osmotic shock (0.1 MPa), the turgor threshold was decreased in two minutes. In addition, the growth never ceased but after an initial drop the initial growth rate and turgor were re-established in less than 10 min [Frensch and Hsiao, 1995] indicating that osmotic adjustment (that restores turgor) took place in a short time scales, again within a frame of 10 minutes.

In our experiment, the recorded wall tension drop induced by contact forces inferior to  $F_N = 0.04 N$  corresponds to a turgor drop lower than 0.05 MPa (calculated with  $F_N/\pi R^2$ ). According to [Frensch and Hsiao, 1995], we can suppose that an osmotic adjustment could have occurred after 10 minutes, increasing turgor and at least partially cancelling the effect of the contact force on the root growth velocity. Osmotic adjustment in response to impedance/external force was already evidenced in Greacen and Oh (1972) [Greacen and Oh, 1972] and Atwell and al. (1988) [Atwell, 1988]). Cell turgor pressure was shown to be strongly increased in response to growth blockage by an axial force [Clark et al., 1996] but without indication on the short term dynamics. Turgor pressure was however not measured and untangling the role of cell wall loosening versus osmoregulation would call for experiments where force is maintained constant by controlling the displacement of the obstacle during the growth. The transition toward longer term mecanoperceptive responses which also tend to slow-down growth [Coutand and Moulia, 2000] could also be studied.

Directional methods to test Lockhart growth by stretching organs with small

weights were first developed as an alternative to measure plastic deformation associated to growth of soybean stem [Nonami and Boyer, 1990b] and proved to be numerically equivalent to non-directional methods [Nonami and Boyer, 1990a]. The method was refined to estimate easily both yield threshold and extensibility of maize leaves after exposure to salinity [Cramer and Bowman, 1991]. Compression experiments of stem pieces (coined "External Force method") were carried out by Cosgrove [Cosgrove, 1987] to study the dynamics of the turgor-growth relationship but "the pattern of force were highly variable" and the technique non pursued. In the light of our experiments it was probably due to the variability of the buckling threshold. Our study is thus the first proof of the equivalence between non-directional and directional methods for plants in the case of compression: parameters estimated with a non-directional method [Frensch and Hsiao, 1995], an hyperosmotic treatment, can predict quantitatively the response of the *EER* distribution ( $L_{GZ}$  and  $EER_{max}$ ) to a directional solicitation, the contact with an obstacle (Figure 9). This model illustrates the power and limitations of the analogy between cell wall growth and rheology to make predictive models of plant tissues with complex growth patterns: the yield threshold distribution inferred from the pre-contact kinematics and the extensibility are sufficient parameters to describe the ten first minutes of the interactions with an obstacle.

## 5 Conclusion

As a conclusion, we built a model experimental system to study how an external mechanical stress impacts the primary growth of the maize radicle. We coupled force and kinematics measurements to investigate the first stages of the root apex contacting a stiff obstacle. We established the force-velocity relationship and characterized fine kinematics parameters such as the growth zone extent and the maximum strain rate. We proposed a derived Lockhart model to take into account the compression force produced by the axial growth against the obstacle. Through this model and by using parameters of the literature for maize roots submitted to water stresses (non-directional methods), we could predict without any adjustable parameter the decrease of velocity and growth zone lengths with force, within the first ten minutes of contact. These results suggest a strong similarity of the early growth responses elicited either by a directional stress (contact) or by an isotropic perturbation (hyperosmotic bath).

## 6 Funding

M.B. Bogeat-Triboulot was supported by a grant overseen by the French National Research Agency (ANR) as part of the "Investissements d'Avenir" program (ANR-11-LABX-0002-01, Lab of Excellence ARBRE). E. Couturier was supported by AnAdSpi ANR-20-CE30-0005-01.

## References

- Bj Atwell. Physiological-Responses of Lupin Roots to Soil Compaction. *Plant and Soil*, 111(2):277–281, October 1988. ISSN 0032-079X. doi: 10.1007/BF02139953. (doi : 10.1007/BF02139953).
- Tobias I. Baskin. Patterns of root growth acclimation: constant processes, changing boundaries. *Wiley Interdisciplinary Reviews-Developmental Biology*, 2(1):65–73, February 2013. ISSN 1759-7684. doi: 10.1002/wdev.94. (doi : 10.1002/wdev.94).
- Renaud Bastien, David Legland, Marjolaine Martin, Lucien Fregosi, Alexis Peaucelle, Stephane Douady, Bruno Moulia, and Herman Hoefte. KymoRod: a method for automated kinematic analysis of rod-shaped plant organs. *Plant Journal*, 88(3):468–475, November 2016. ISSN 0960-7412. doi: 10.1111/tpj.13255. (doi : 10.1111/tpj.13255).
- A. G. Bengough, C. Croser, and J. Pritchard. A biophysical analysis of root growth under mechanical stress. *Plant and Soil*, 189(1):155–164, February 1997. ISSN 0032-079X. doi: 10.1023/A:1004240706284. (doi : 10.1023/A:1004240706284).
- A. Glyn Bengough, B. M. McKenzie, P. D. Hallett, and T. A. Valentine. Root elongation, water stress, and mechanical impedance: a review of limiting stresses and beneficial root tip traits. *Journal of Experimental Botany*, 62(1):59–68, January 2011. ISSN 0022-0957. doi: 10.1093/jxb/erq350. (doi : 10.1093/jxb/erq350).
- Francois Bizet, A. Glyn Bengough, Irene Hummel, Marie-Beatrice Bogeat-Triboulot, and Lionel X. Dupuy. 3D deformation field in growing plant roots reveals both mechanical and biological responses to axial mechanical forces. *Journal of Experimental Botany*, 67(19):5605–5614, October 2016. ISSN 0022-0957. doi: 10.1093/jxb/erw320. (doi : 10.1093/jxb/erw320).
- L. J. Clark, W. R. Whalley, A. R. Dexter, P. B. Barraclough, and R. A. Leigh. Complete mechanical impedance increases the turgor of cells in the apex of pea roots. *Plant Cell and Environment*, 19(9):1099–1102, September 1996. ISSN 0140-7791. doi: 10.1111/j.1365-3040.1996.tb00217.x. (doi : 10.1111/j.1365-3040.1996.tb00217.x).
- L. J. Clark, A. G. Bengough, W. R. Whalley, A. R. Dexter, and P. B. Barraclough. Maximum axial root growth pressure in pea seedlings: effects of measurement techniques and cultivars. *Plant and Soil*, 209(1): 101–109, 1999. ISSN 0032-079X. doi: 10.1023/A:1004568714789. (doi : 10.1023/A:1004568714789).
- Tino Colombi and Thomas Keller. Developing strategies to recover crop productivity after soil compaction-A plant eco-physiological perspective. *Soil*

- £ Tillage Research*, 191:156–161, August 2019. ISSN 0167-1987. doi: 10.1016/j.still.2019.04.008. (doi : 10.1016/j.still.2019.04.008).
- Dj Cosgrove. Wall Relaxation and the Driving Forces for Cell Expansive Growth. *Plant Physiology*, 84(3):561–564, July 1987. ISSN 0032-0889. doi: 10.1104/pp.84.3.561. (doi : 10.1104/pp.84.3.561).
- C. Coutand and B. Moulia. Biomechanical study of the effect of a controlled bending on tomato stem elongation: local strain sensing and spatial integration of the signal. *Journal of Experimental Botany*, 51(352):1825–1842, November 2000. ISSN 0022-0957. doi: 10.1093/jexbot/51.352.1825. (doi : 10.1093/jexbot/51.352.1825).
- Gr Cramer and Dc Bowman. Kinetics of Maize Leaf Elongation .1. Increased Yield Threshold Limits Short-Term, Steady-State Elongation Rates After Exposure to Salinity. *Journal of Experimental Botany*, 42(244):1417–1426, November 1991. ISSN 0022-0957. doi: 10.1093/jxb/42.11.1417. (doi : 10.1093/jxb/42.11.1417).
- Rosemary J. Dyson, Gema Vizcay-Barrena, Leah R. Band, Anwasha N. Fernandes, Andrew P. French, John A. Fozard, T. Charlie Hodgman, Kim Kenobi, Tony P. Pridmore, Michael Stout, Darren M. Wells, Michael H. Wilson, Malcolm J. Bennett, and Oliver E. Jensen. Mechanical modelling quantifies the functional importance of outer tissue layers during root elongation and bending. *New Phytologist*, 202(4):1212–1222, June 2014. ISSN 0028-646X. doi: 10.1111/nph.12764. (doi : 10.1111/nph.12764).
- J. Frensch and Tc Hsiao. Transient Responses of Cell Turgor and Growth of Maize Roots as Affected by Changes in Water Potential. *Plant Physiology*, 104(1):247–254, January 1994. ISSN 0032-0889. doi: 10.1104/pp.104.1.247. (doi : 10.1104/pp.104.1.247).
- J. Frensch and Tc Hsiao. Rapid Response of the Yield Threshold and Turgor Regulation During Adjustment of Root-Growth to Water-Stress in Zea-Mays. *Plant Physiology*, 108(1):303–312, May 1995. ISSN 0032-0889. doi: 10.1104/pp.108.1.303. (doi : 10.1104/pp.108.1.303).
- Barry Gardiner, Peter Berry, and Bruno Moulia. Review: Wind impacts on plant growth, mechanics and damage. *Plant Science*, 245:94–118, April 2016. ISSN 0168-9452. doi: 10.1016/j.plantsci.2016.01.006. (doi : 10.1016/j.plantsci.2016.01.006).
- W. Gill and G. Bolt. Pfeffer’s Studies of the Root Growth Pressures Exerted by Plants. 1955. doi: 10.2134/AGRONJ1955.00021962004700040004X. (doi : 10.2134/AGRONJ1955.00021962004700040004X).
- El Greacen and Js Oh. Physics of Root Growth. *Nature-New Biology*, 235(53): 24–&, 1972. doi: 10.1038/newbio235024a0. (doi : 10.1038/newbio235024a0).



- Pb Green, Ro Erickson, and J. Buggy. Metabolic and Physical Control of Cell Elongation Rate - in-Vivo Studies in Nitella. *Plant Physiology*, 47(3):423–&, 1971. ISSN 0032-0889. doi: 10.1104/pp.47.3.423. (doi : 10.1104/pp.47.3.423).
- Peter J. Gregory. *Plant Roots: Growth, Activity and Interactions with the Soil*. Blackwell Publishing Ltd, 2006. ISBN 978-1-4051-1906-1. (doi : 10.1002/9780470995563).
- Peter J. Gregory, A. Glyn Bengough, Dmitri Grinev, Sonja Schmidt, W. Thomas, Tobias Wojciechowski, and Iain M. Young. Root phenomics of crops: opportunities and challenges. *Functional Plant Biology*, 36(10-11):922–929, 2009. ISSN 1445-4408. doi: 10.1071/FP09150. (doi : 10.1071/FP09150).
- Marcus Griffiths, Benjamin M. Delory, Vanessa Jawahir, Kong M. Wong, G. Cody Bagnall, Tyler G. Dowd, Dmitri A. Nusinow, Allison J. Miller, and Christopher N. Topp. Optimisation of root traits to provide enhanced ecosystem services in agricultural systems: A focus on cover crops. *Plant Cell and Environment*, 45(3):751–770, March 2022. ISSN 0140-7791. doi: 10.1111/pce.14247. (doi : 10.1111/pce.14247).
- Kemo Jin, Jianbo Shen, Rhys W. Ashton, Ian C. Dodd, Martin A. J. Parry, and William R. Whalley. How do roots elongate in a structured soil? *Journal of Experimental Botany*, 64(15):4761–4777, November 2013. ISSN 0022-0957. doi: 10.1093/jxb/ert286.
- Evelyne Kolb, Valerie Legue, and Marie-Beatrice Bogeat-Triboulot. Physical root-soil interactions. *Physical Biology*, 14(6):065004, December 2017. ISSN 1478-3967. doi: 10.1088/1478-3975/aa90dd. (doi : 10.1088/1478-3975/aa90dd).
- Benoit Landrein and Gwyneth Ingram. Connected through the force: mechanical signals in plant development. *Journal of Experimental Botany*, 70(14):3507–3519, July 2019. ISSN 0022-0957. doi: 10.1093/jxb/erz103. (doi : 10.1093/jxb/erz103).
- Ja Lockhart. An Analysis of Irreversible Plant Cell Elongation. *Journal of Theoretical Biology*, 8(2):264–&, 1965. ISSN 0022-5193. doi: 10.1016/0022-5193(65)90077-9. (doi : 10.1016/0022-5193(65)90077-9).
- Jonathan P. Lynch, Sacha J. Mooney, Christopher F. Strock, and Hannah M. Schneider. Future roots for future soils. *Plant Cell and Environment*, 45(3):620–636, March 2022. ISSN 0140-7791. doi: 10.1111/pce.14213. (doi : 10.1111/pce.14213).
- H. Nonami and Js Boyer. Primary Events Regulating Stem Growth at Low Water Potentials. *Plant Physiology*, 93(4):1601–1609, August 1990a. ISSN 0032-0889. doi: 10.1104/pp.93.4.1601. (doi : 10.1104/pp.93.4.1601).

- H. Nonami and Js Boyer. Wall Extensibility and Cell Hydraulic Conductivity Decrease in Enlarging Stem Tissues at Low Water Potentials. *Plant Physiology*, 93(4):1610–1619, August 1990b. ISSN 0032-0889. doi: 10.1104/pp.93.4.1610. (doi : 10.1104/pp.93.4.1610).
- Winfried S. Peters and Tobias I. Baskin. Tailor-made composite functions as tools in model choice: the case of sigmoidal vs bi-linear growth profiles. *Plant Methods*, 2:11, 2006. doi: 10.1186/1746-4811-2-11. (doi : 10.1186/1746-4811-2-11).
- W. Pfeffer. *Druck- und Arbeitsleistung durch wachsende Pflanzen*. S. Hirzel,, Leipzig,, 1893. ISBN DOI: 10.5962/bhl.title.13148. (doi : 10.5962/bhl.title.13148).
- Liyana Popova, Dagmar van Dusschoten, Kerstin A. Nagel, Fabio Fiorani, and Barbara Mazzolai. Plant root tortuosity: an indicator of root path formation in soil with different composition and density. *Annals of Botany*, 118(4): 685–698, October 2016. ISSN 0305-7364. doi: 10.1093/aob/mcw057. (doi : 10.1093/aob/mcw057).
- Izabela Potocka and Joanna Szymanowska-Pulka. Morphological responses of plant roots to mechanical stress. *Annals of Botany*, 122(5):711–723, October 2018. ISSN 0305-7364. doi: 10.1093/aob/mcy010. (doi : 10.1093/aob/mcy010).
- J. Pritchard. The Control of Cell Expansion in Roots. *New Phytologist*, 127(1): 3–26, May 1994. ISSN 0028-646X. doi: 10.1111/j.1469-8137.1994.tb04255.x. (doi : 10.1111/j.1469-8137.1994.tb04255.x).
- Ruben Rellan-Alvarez, Guillaume Lobet, and Jose R. Dinneny. Environmental Control of Root System Biology. In S. S. Merchant, editor, *Annual Review of Plant Biology, Vol 67*, volume 67, pages 619–642. Annual Reviews, Palo Alto, 2016. ISBN 978-0-8243-0667-0. (doi : 10.1146/annurev-arplant-043015-111848).
- Re Sharp, Wk Silk, and Tc Hsiao. Growth of the Maize Primary Root at Low Water Potentials .1. Spatial-Distribution of Expansive Growth. *Plant Physiology*, 87(1):50–57, May 1988. ISSN 0032-0889. doi: 10.1104/pp.87.1.50. (doi : 10.1104/pp.87.1.50).
- Wk Silk and Ro Erickson. Kinematics of Plant-Growth. *Journal of Theoretical Biology*, 76(4):481–501, 1979. ISSN 0022-5193. doi: 10.1016/0022-5193(79)90014-6. (doi : 10.1016/0022-5193(79)90014-6).
- N. Souty. Mechanical-Behavior of Growing Roots .1. Measurement of Penetration Force. *Agronomie*, 7(8):623–630, 1987. ISSN 0249-5627. doi: 10.1051/agro:19870810. (doi : 10.1051/agro:19870810).

- Christopher J. Stubbs, Douglas D. Cook, and Karl J. Niklas. A general review of the biomechanics of root anchorage. *Journal of Experimental Botany*, 70 (14):3439–3451, July 2019. ISSN 0022-0957. doi: 10.1093/jxb/ery451. (doi : 10.1093/jxb/ery451).
- Saoirse R. Tracy, Colin R. Black, Jeremy A. Roberts, and Sacha J. Mooney. Soil compaction: a review of past and present techniques for investigating effects on root growth. *Journal of the Science of Food and Agriculture*, 91 (9):1528–1537, July 2011. ISSN 0022-5142. doi: 10.1002/jsfa.4424. (doi : 10.1002/jsfa.4424).
- Bw Veen and Fr Boone. The Influence of Mechanical Resistance and Soil-Water on the Growth of Seminal Roots of Maize. *Soil & Tillage Research*, 16(1-2): 219–226, April 1990. ISSN 0167-1987. doi: 10.1016/0167-1987(90)90031-8. (doi : 10.1016/0167-1987(90)90031-8).
- A. Walter, R. Feil, and U. Schurr. Expansion dynamics, metabolite composition and substance transfer of the primary root growth zone of *Zea mays* L. grown in different external nutrient availabilities. *Plant Cell and Environment*, 26 (9):1451–1466, September 2003. ISSN 0140-7791. doi: 10.1046/j.0016-8025.2003.01068.x. (doi : 10.1046/j.0016-8025.2003.01068.x).
- Chvan Youssef, Francois Bizet, Renaud Bastien, David Legland, Marie-Beatrice Bogeat-Triboulot, and Irene Hummel. Quantitative dissection of variations in root growth rate: a matter of cell proliferation or of cell expansion? *Journal of Experimental Botany*, 69(21):5157–5168, October 2018. ISSN 0022-0957. doi: 10.1093/jxb/ery272. (doi : 10.1093/jxb/ery272).
- Gl Zhu and Js Boyer. Enlargement in Chara Studied with a Turgor Clamp - Growth-Rate Is Not Determined by Turgor. *Plant Physiology*, 100(4):2071–2080, December 1992. ISSN 0032-0889. doi: 10.1104/pp.100.4.2071. (doi : 10.1104/pp.100.4.2071).